ELSEVIER

Contents lists available at ScienceDirect

Journal of Sound and Vibration

journal homepage: www.elsevier.com/locate/jsvi



Ferroelectret nanogenerators for loudspeaker applications: A comprehensive study



Henry Dsouza ^a, Andre Van Schyndel ^b, Juan Pastrana ^a, Yunqi Cao ^a, Eric Hunter ^c, Brad Rakerd ^c, Nelson Sepúlveda ^{a,*}

- ^a Department of Electrical and Computer Engineering, Michigan State University, East Lansing, MI, United States
- ^b Ford Motor Company, Dearborn, MI, United States
- ^c Department of Communicative Sciences and Disorders, Michigan State University, East Lansing, MI, United States

ARTICLE INFO

Article history: Received 25 June 2019 Revised 7 November 2019 Accepted 15 November 2019 Available online 18 November 2019 Handling Editor: S. Felix

Keywords: Flexible electronics Self-powered loudspeaker Directivity

ABSTRACT

A ferroelectret nanogenerator (FENG) was recently developed as a flexible energy harvesting device with bi-directional capability between electrical and mechanical energy domains, and its use as a loudspeaker/microphone was demonstrated. Dependencies of Sound Pressure Levels (SPLs) generated by FENG due to an AC voltage stimulus, surface area, geometric shape, and addition of layers are presented here. Also, the relation between the sound output to the electrical input is studied and shown to be linear, which demonstrates that these flexible loudspeakers have low distortion within the human audible range of 20 Hz to 20 kHz. A study for ultrasonic frequencies up to 40 kHz is also presented. A theoretical model relating the electrical and acoustical domain of the FENG is developed based on the experimental observations made and using Boundary Element Methods (BEM) to accurately mimic the testing environment for simulation purposes. The comparison between this model and the actual behavior is presented under several cases and observed to be closely correlated.

© 2019 Elsevier Ltd. All rights reserved.

1. Introduction

Audiovisual technologies are driven by convenience and immersive experience (e.g. virtual and augmented reality). This trend dictates the path for future advancements in consumer electronics and drives the interest in the science that makes possible its progress. In particular, size and flexibility are parameters that are being heavily considered at the time of determining convenience and experience enhancement. Wearable/concealable products are becoming the most sought after amidst the other pocket friendly technology. Improving human/system connectivity and interfaces requires the optimal use of the senses. Visual components and haptic devices have been key players for many years [1,2]. Auditory sensing should also be part of an inclusive system that allows for an immersive experience; and having it in flexible form, compatible with wearable electronics is vital. To have a loudspeaker embedded within the thin lining of wearable clothes is certainly a motivating prospect [3], or even loudspeakers that can be attached to human skin [4]. Scientific advances in thin film, flexible acoustic actuators is crucial for technological progress of human-system interactions in multiple applications, such as electronic papers, virtual reality [5], and wearable electronics for the above mentioned auditory systems [6,7].

Traditional electrodynamic loudspeakers use a coil and a diaphragm. Electrical signals are fed to a voice coil which actuates a diaphragm to produce sound waves. This set-up is known to have a relatively large footprint, mainly due to the required

E-mail address: nelsons@egr.msu.edu (N. Sepúlveda).

^{*} Corresponding author.

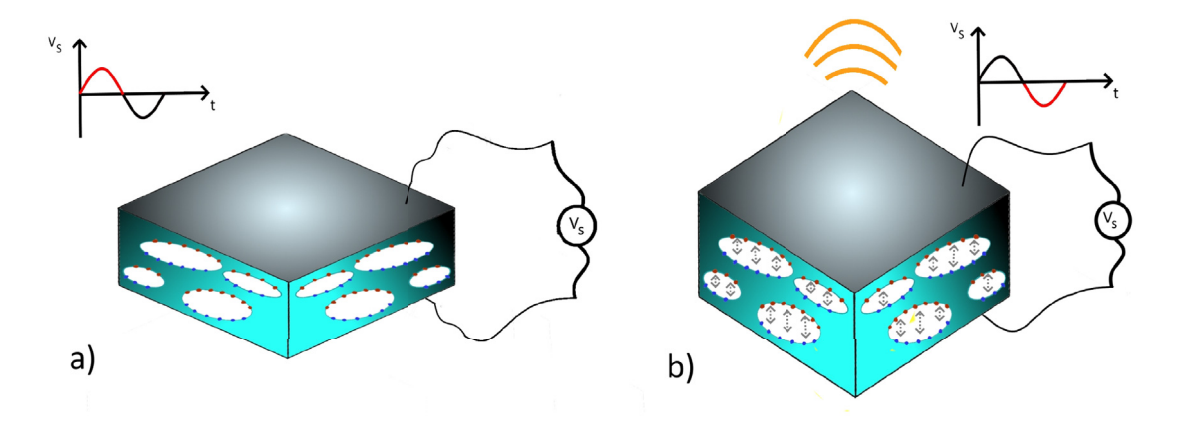


Fig. 1. Shows the operating principle of the FENG. a) Shows the positive half cycle of the AC voltage applied which causes the FENG to compress and b) shows the negative half cycle of the voltage which causes the FENG to expand.

magnets, making it unlikely to be flexible and compatible with wearable electronics [8,9]. This led to research on the creation and study of sensitive, flexible piezoelectric materials for energy harvesting/sensors/actuators [10], with particular relevance on thin-film sensors and acoustic actuators [11]. The applications of thin film acoustic materials are very wide spread. For instance, growth in population has led to house construction close to highways and airports, and windows are the primary path through which noise from such places enters a house. Thin film acoustic materials can work as a transparent flat-panel loudspeaker/microphone and achieve noise cancellation [12–17]. Moreover, microphones/loudspeakers are necessary in voice-activated electronics; where size and flexibility also play an important role [18,19].

Recently, applications for flexible acoustic actuators has been revolutionized with the triboelectric nanogenerator (TENG) technology which provides the basis for robotic auditory systems [20]. Other nanogenerators (NGs) based on polypropylene ferroelectrets (PPFE) were demonstrated to be flexible, foldable, and promising devices for self-powered systems [21,22].

In this work, we present experimental data for FENG output as a function of area, FENG's frequency response, directivity, effect of folding and harmonic distortion. The experimental setup is described, and a theoretical model based on boundary element methods (BEM) is presented; which validates the frequency response and directivity measurements of different shapes.

2. Experimental setup

Fig. 1 shows the device cross-section, which includes artificial voids created inside the foam structure by means of microplasma discharging. These voids form numerous dipoles, which allows for transducers made from this material to be highly sensitive to an electrical stimulus that generates contraction/expansion across the device's thickness. The contraction/expansion of the device's surface will follow the time response of the input electric signal, and thus generate pressure variations in the surrounding medium and sound waves.

Due to the material's bi-directional energy conversion capability (i.e. its capacity to convert mechanical to electrical energy and vice-versa), early research on FENG devices has focused on energy harvesting applications. Examples of this work include applications in illumination, liquid crystal display (LCD) and a self-powered keyboards [21]. Next steps to advance this technology include the study of these materials based on the figure of merit which is peculiar to a given application, and to develop theoretical models in the specific targeted domain. Such models will serve as an important tool at designing end applications using these devices. Hence, the focus of the present work is to understand how the physical parameters such as shape, size and thickness correlate to the acoustic output (sound pressure levels and directivity) of FENG devices, due to electrical input actuation. A detailed study with steady trends and backing with computational model simulations is included.

All the experiments were performed inside an anechoic chamber as shown in Fig. 2. This chamber was characterized by Brad Rakerd [23]. The FENG and sensing microphone were held in the middle using low profile stands, clamps and pedestals. Electrical connections extend from the outside of the chamber to the FENG and microphone inside the chamber via feedthroughs that have minimal disruption to the absorbing cone array. A 1/2" pre-polarized free field microphone with a sensitivity of 12.6 mV/Pa and frequency range ($\pm 3 \text{ dB}$) from 3.15 to 40000 Hz (378A06, PCB Inc.) was used to record/measure the pressure changes created by the FENG, as shown in Fig. 2. The microphone was connected to a signal conditioner 484B06, PCB Inc. The FENG is placed on a 0.5 inch thick MDF board ($13 \text{ cm} \times 16 \text{ cm}$) using double-sided tape having an area density of 13.17 mg/cm^2 . This board is held in place using a pedestal and a clamp as shown in Fig. 2.

3. Parameters of interest and measurements

To design a loudspeaker using a FENG, it is necessary to find the parameters that are most influential in the device's acoustic response. This will not only lead to a better understanding of the device's operation, but also identify the variables that can be

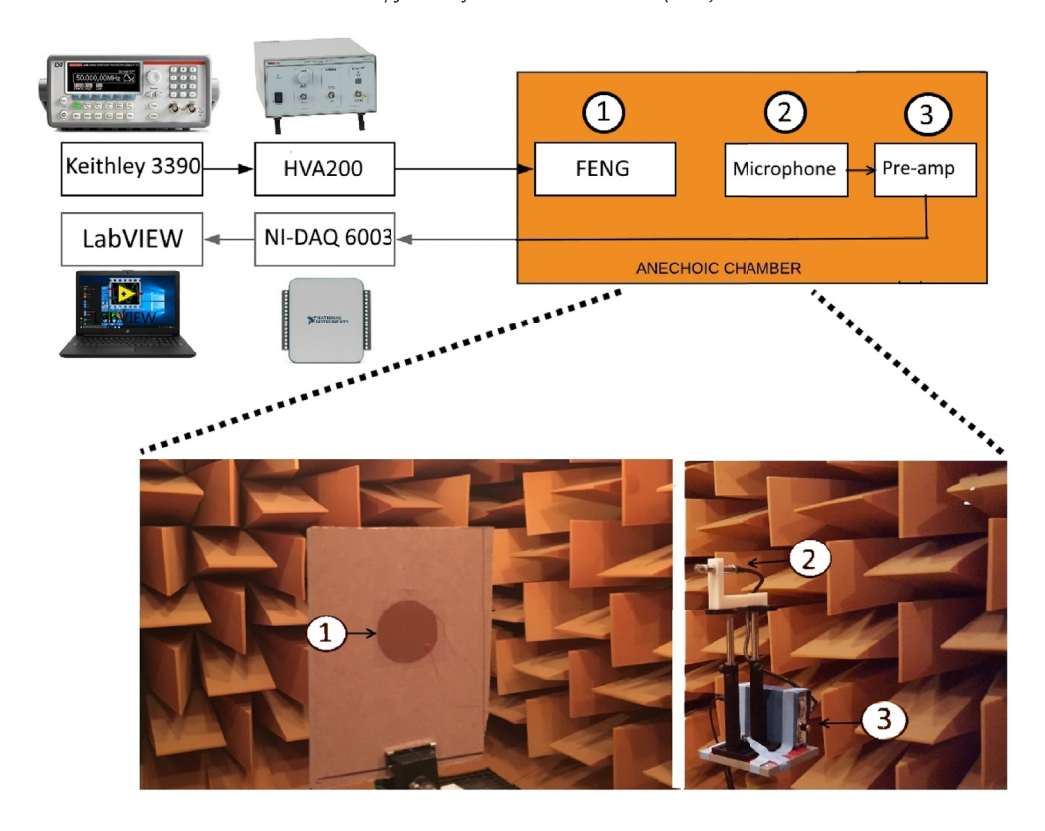


Fig. 2. Shows the schematic diagram of the test setup. The FENG, microphone and the pre-amp are placed inside the anechoic chamber as shown in the expanded view. The MDF board on which the FENG (circle in this instance) is fixed measures 16 cm × 13 cm x 1.27 cm.

controlled during the device preparation that will be most influential on different performance metrics as a loudspeaker. To this end, our first set of experiments were designed to characterize FENG devices with different parameters and study their role on different performance metrics. Factors such as device surface area, folding effects, and directivity with respect to different shapes and mounting surfaces were studied. The previous proof-of-concept work done on FENG devices as microphone/loudspeakers was focused on a functionality demonstration, and did not involve testing environments that could allow for the study of individual parameters on the device's response. Therefore, a comprehensive characterization of the device, and the derivation of theoretical models that validate the device's functionality and describe the system were not possible [24]. In this work, a systematic approach is used to allow for a detailed study of FENG devices as loudspeakers. For example, all the experiments in this work are done in an acoustic anechoic chamber with absorbing cones (1 m long) on all the 6 faces of the chamber, which eliminates reflections from surrounding surfaces during testing, even for low frequencies in the human audible range. Also, FENG layers were firmly fixed to each other, thus eliminating the possibility of air pockets between layers, which affects Sound Pressure Level (SPL) output and directivity. All the testing set-up improvements made in this work allowed for a theoretical model that helps explain the use of FENG devices as loudspeakers and establishes a design platform for future designs with specific performance requirements.

3.1. Area vs. sound pressure level

SPL or acoustic pressure level is a logarithmic measure of the effective pressure of a sound relative to a reference value,

$$SPL = 20\log_{10}\left(\frac{P}{P_o}\right). \tag{1}$$

In this case this reference value (P_o) is taken as the threshold for human hearing of 20 μ Pa at 1 kHz. FENG devices were fabricated with different surface area and shapes, maintaining the thickness as a constant parameter. Nonetheless, a single FENG was used and cut down into pieces of different surface areas to measure the SPL output. This was done to limit the number of varying process parameters during the manufacturing of the FENG to only differences in area and shape. The FENG devices used as loudspeakers in this work were 9 cm², 16 cm² and 64 cm², fixed on an MDF board and held in place using a bracket. The microphone was placed at 30 cm from the FENG and aligned to the center of the FENG geometry. An AC signal of 127 V_{rms} was supplied to the FENG and the output was recorded using the microphone. The recorded data was sampled using a NI-DAQ 6003 at a sample rate of 100 KSPS (which sets the Nyquist frequency above our highest measured frequency). A Fast Fourier

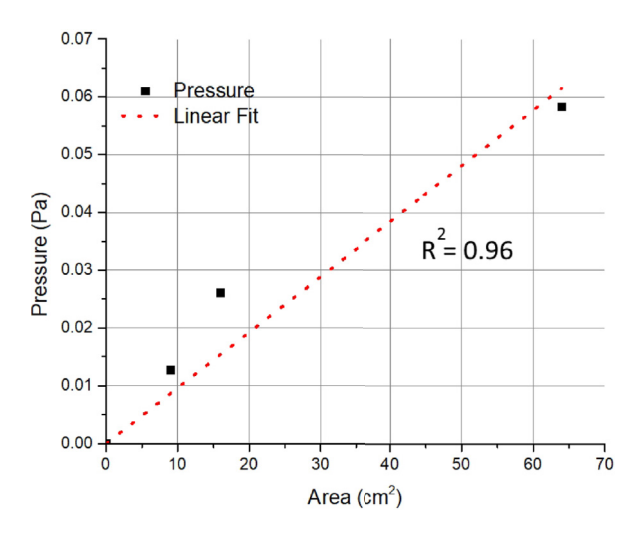


Fig. 3. Sound pressure generated by FENG with respect to area. Linear Fit ($R^2 = 0.96$) is shown.

Transform (FFT) was performed on the sampled data through LabVIEW. Frequency bins of interest were identified (depending on the experiment), the power level was determined and converted to pressure, representing the force exerted per unit area on the microphone diaphragm due the acoustic waves created by the FENG's contraction and expansion movements. The frequency of the input signal was swept from 100 Hz to 20 kHz. Flat-weighted sound level measurements of the background noise level in the anechoic chamber show that the noise had most of its power in the lower frequencies and settles to a minimum after 2 kHz [23]. Thus points until 2 kHz were neglected due to poor signal-to-noise ratio (SNR). The average of pressure values between 2 and 20 kHz is recorded. The same procedure was applied to a FENG of 9 cm² and 16 cm².

Plotting pressure (averaged between 2 and 20 kHz) as a function of area as shown in Fig. 3; reveals that the sound pressure increases approximately linearly with area.

3.2. Linearity

The term "distortion" is used to refer to any change in a signal upon conversion from the electrical to the acoustical domain. When the input signal is sinusoidal, "harmonic distortion" specifically refers to the strength of spurious signals which are integral multiples of the input frequency. A nonlinear input to output relation can cause harmonic distortion, in this case between voltage and sound pressure. An ideal loudspeaker is expected to have zero distortion i.e the output (sound pressure) will scale linearly with the input voltage. In order to study this, the test was carried out on the four layered FENG but varying the input voltage in steps of 12.5 V from 12.5 V_{rms} to 127 V_{rms} . As seen in Fig. 4, the multi-structural device exhibits linear behavior. The spectrum of the output voltage of the microphone when the FENG was excited at 2000 Hz in the form of a Fast Fourier Transform (FFT) is shown in Fig. 5.

3.3. Directivity of the FENG

The term "frequency response" refers to the variation in SPL with changes in frequency. The "directivity" describes how a loudspeaker sends sound waves in different directions. The theoretical model for an omnidirectional sound source consists of a pulsating sphere that radiates from a point in space. For a finite sized source, the evenness of the dispersion in all directions is a function of the characteristic size of the source. The dispersion of the source narrows at frequencies for which the wavelength approaches or is smaller than the characteristic dimension of the source. A wide directivity loudspeaker maintains amplitude consistency between the on-axis (perpendicular to the loudspeaker diaphragm plane) and off-axis (at a direction 90° from the on-axis) as seen in Fig. 6. Narrow directivity loudspeakers, on the other hand, change their amplitudes substantially between the axes. Diffraction, shading and interference in the sound waves around the loudspeaker and its associated cabinetry produce lobes at different frequencies. Thus, it is important to know how directional a loudspeaker made from FENG will be. In the same manner as previous experiments, FENG of different shapes and orientations were cut and fixed on the MDF board using double-sided tape. The MDF board was mounted on a rotatable clamp such that it can be turned and the angle in reference with the microphone can be measured as shown in Fig. 6 (the oval shape was rotated along its longer axis and the strip was rotated along its shorter side). The microphone was placed 30 cm from the geometric center of the FENG. A time-varying voltage signal of 127 V_{rms}, with frequencies ranging from 100 Hz to 20 kHz is sent to the two electrodes of the FENG. The sound levels were recorded by the microphone and sampled by the Ni-DAQ6003. Fig. 7 shows the polar plots for 5, 10, 15 and 20 kHz. Only half of the polar plot is shown. The other half is symmetric about the on-axis, both in the DUT and also the testing environment. A

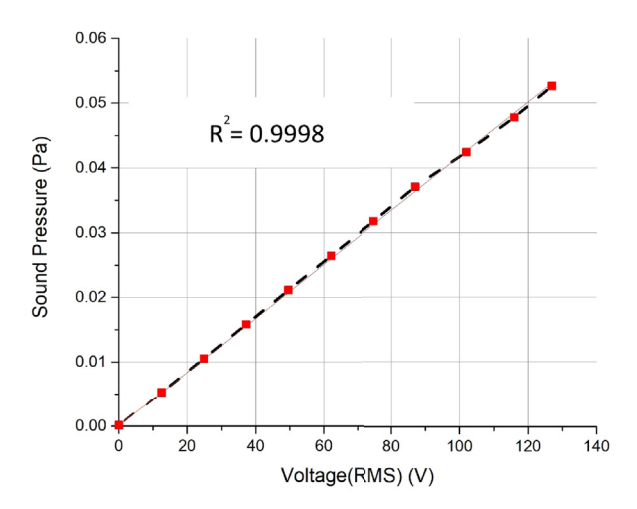


Fig. 4. The change in sound pressure (averaged between 2 and 20 kHz) for different voltage levels is plotted and shown to be linear. The R² value is shown in the graph which represents the deviation from ideal linear behavior.

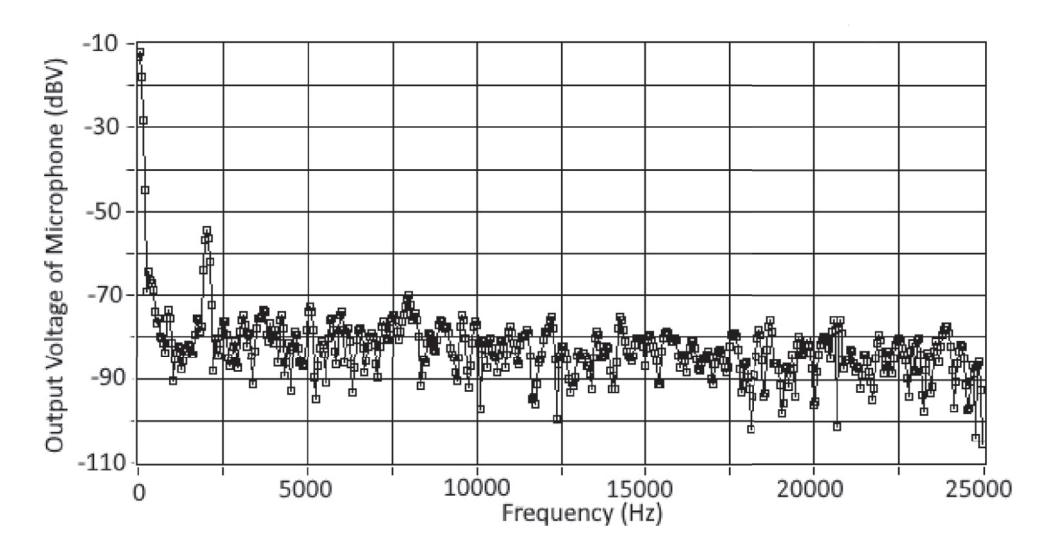


Fig. 5. Spectrum of acoustic pressure at 2000 Hz for a square FENG of side 4 cm, observed from 30 cm, excited with 127 V_{rms} .

higher intensity is observed on on-axis, in front of the FENG as compared to behind the back-plate. This is expected since the MDF board attenuates the sound waves with wavelengths comparable to or smaller than the side length of the board.

Although all the shapes have the same surface area, which means that the sound pressure levels exerted by them should be same at 90° (in this case since all the measurements are far field), there is a small variation. One of the reasons for this could be due to the difference in dipole distribution across the volume of the FENG. In this case the FENG that makes up the circle shape has slightly higher output than other shapes. As the frequency increases, it can be observed that the shapes are becoming more directional; i.e the ratio of side lobes to that of 90° decreases. Directivity patterns on these shapes will further help validate the developed model in later sections.

3.4. Frequency response and effect of folding

FENG devices present flexible thin-film characteristics that allows folding and stacking to form a multilayer structure. Li et al. showed that for a stacked multilayer FENG device, the SPL was proportional to the number of layers [24]. The multilayer effect on the output of the device is observed as a function of added layers.

The option of stacking the FENGs and actuating them using a 127 V_{rms} signal is explored. Since double-sided tape was used for the parallel arrangement of the devices, the effect of mass loading was established to account for any attenuation due to the binding method. A single layer of FENG was fixed on the MDF board. As seen in Fig. 8, adding 3 layers of double-sided tape to a FENG's surface does not affect the device's output.

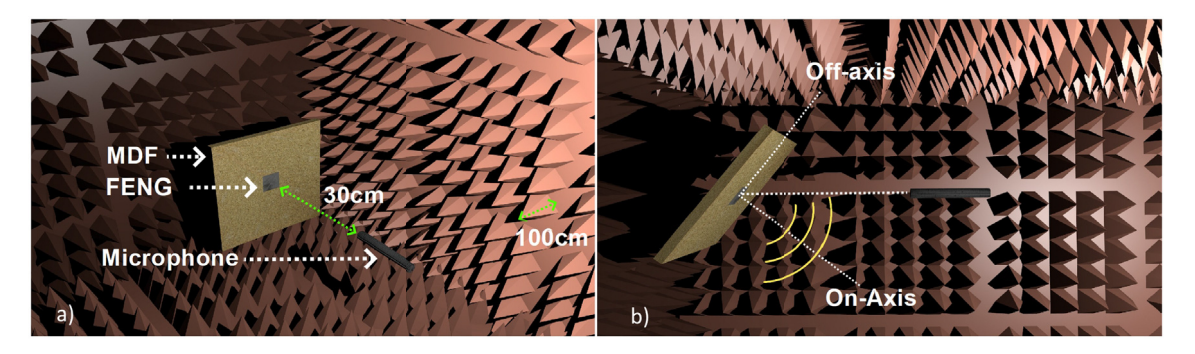


Fig. 6. a) FENG on MDF board and the microphone aligned to the center of the FENG at 30 cm (not to scale). The rest of the setup (including the electrical connections to the FENG) is not shown for clarity; b) One such instance of directivity measurement where the FENG is rotated while microphone kept stationary.

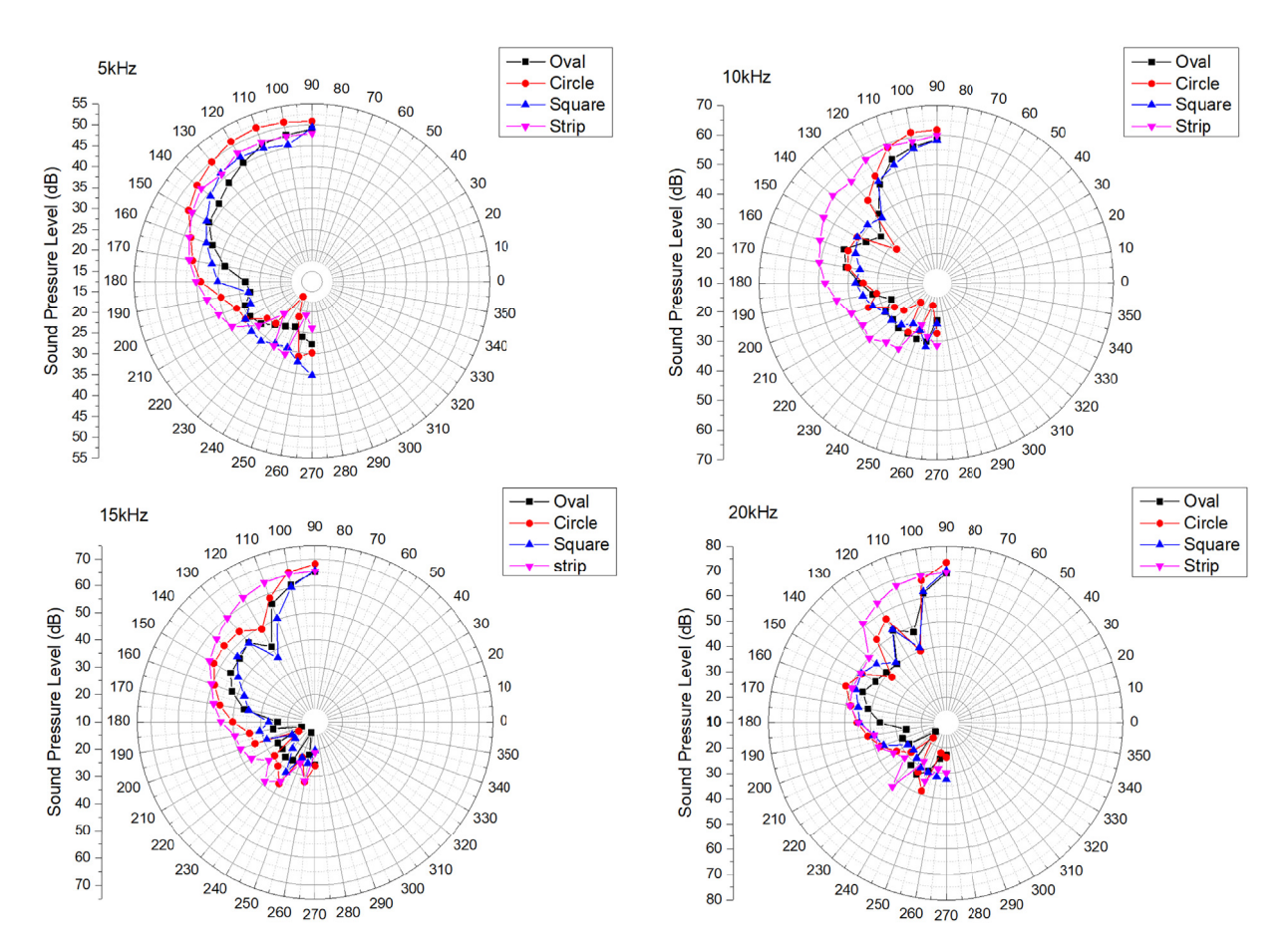


Fig. 7. Directivity of 4 different shapes across 2 quadrants. 90° represents on-axis direction, normal to the MDF in direction to the microphone (see Fig. 6b).

As seen in the above graph, the curves lay on top of each other until % 15 kHz, after which they begin to diverge. This divergence, although small, could be due to the mass loading effect on the resonant frequency (which is beyond audible range). The FENGs are now layered on top of each other as shown in Fig. 9a and electrically connected in parallel to study the effect of layers on sound pressure output. The results are as shown in Fig. 9b. Here the output scaling with each added layer is normalised with the results from the single layer to show the scaling factor, so that the Y-axis in Pascals (Pa) is relative to the response of the single layer FENG.

It is observed that the pressure scales linearly with addition of layers for the FENG acting as a loudspeaker. This property will help reach higher output levels with lower input voltages for excitation.

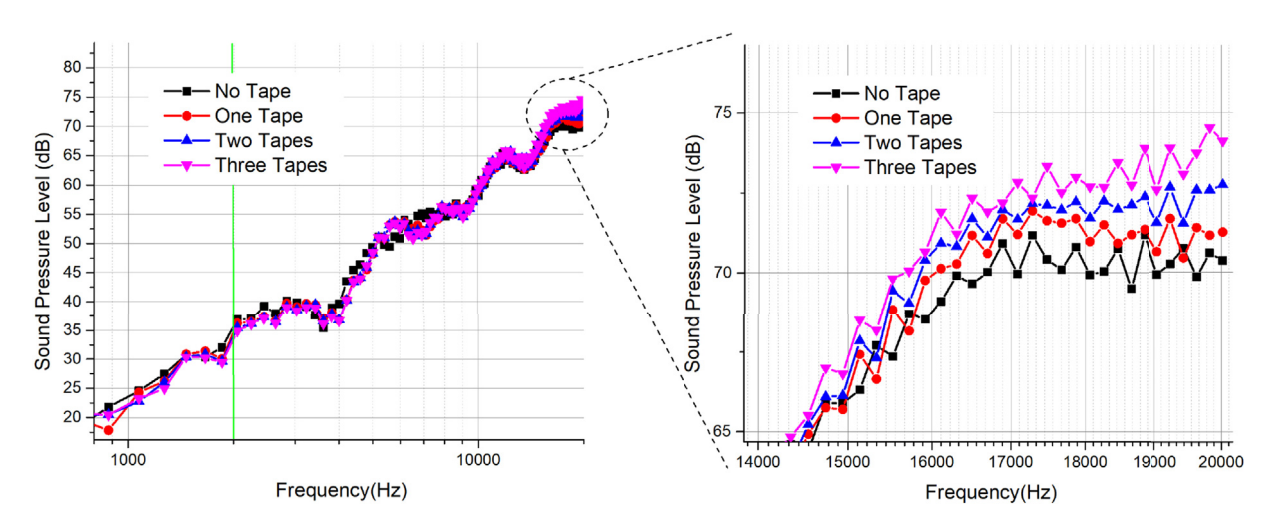


Fig. 8. Frequency response of FENG with increasing number of tapes are stacked over one another (green line marks the 2 kHz point after which the noise levels of the room are the minimum, although measurements where made at frequencies below that). The graph also shows the zoomed in version in the frequency range 13–20 kHz. (For interpretation of the references to color in this figure legend, the reader is referred to the Web version of this article.)

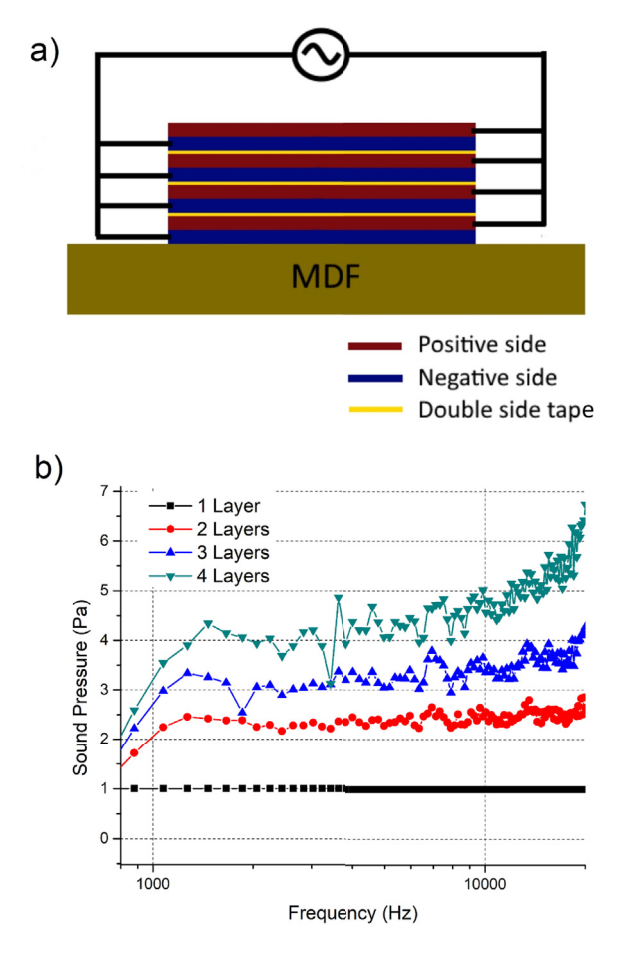


Fig. 9. a) The schematic for electrical connections made to the FENG. b) The output is recorded after addition of every layer across frequency and normalised to a single layer FENG.

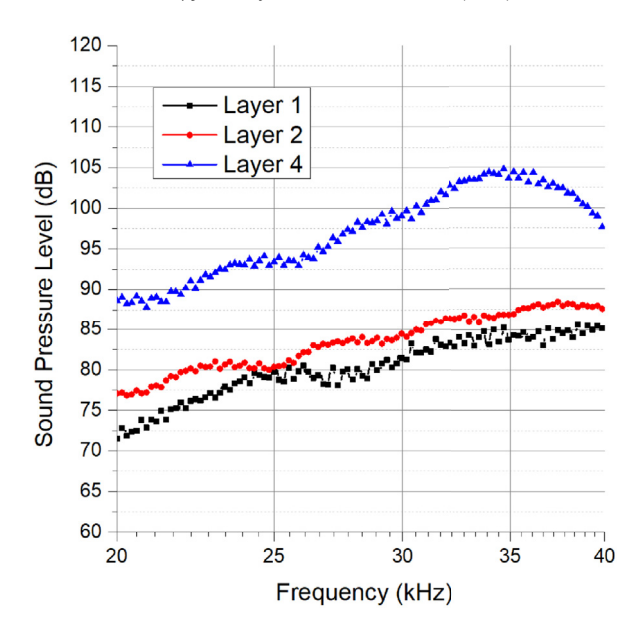


Fig. 10. SPL of FENG in the ultrasound range, along with the trend of addition of layers.

3.5. Ultrasound performance

Operation of the present device in ultrasonic frequencies can broaden its applicability. For example, non-destructive evaluation techniques used in material characterization and structural health monitoring often operate in ultrasonic frequencies [25–27]. The characterization of the present device in ultrasound was done by using 4 cm \times 4 cm (16 cm²) FENGs, which were excited with AC signal of 127 V_{rms} from 20 to 40 kHz. The output is shown in Fig. 10.

The output of a single and two layer FENG continues to rise at 12 dB/octave. The 4 layer FENG has a higher slope until about 35 kHz, at which point it peaks and changes sign. This might be again due to resonance, as discussed in the previous section. This resonance peak is not observed for the single and two layer FENG, since they have lower mass and therefore higher mechanical resonance frequencies.

4. Theoretical modeling and validation

When the FENG experiences an electrical input signal, dipoles expand or contract depending on the potential applied [21]. In turn, mechanical vibrations are generated and are translated as an acoustic wave. A computational model for the FENG can then be assumed to behave as a rigid piston of given shape moving forward and backward, creating the acoustic wave. However, to simulate the previous experimental configuration, a boundary condition must be considered as to represent the FENG fixed to the MDF board. The piston analogy allows to computationally/analytically solve for pressure or particle velocity at given point in space around the FENG. To establish a relation between the FENG's input (electrical signal) and output (displacement), a voltage response definition is introduced.

4.1. Voltage response definition

The assumption of linear change in thickness (D) with applied voltage (V) implies an intrinsic response of the FENG material when used as a loudspeaker:

$$R_{\nu} = \frac{1}{D} \frac{\partial D}{\partial V}.$$
 (2)

The intrinsic response R_v (units of V^{-1}) is the fractional change in FENG thickness per applied Volt. It is expected that R_v would depend on the dipole density and the average charge on the dipoles. The assumption that R_v is constant throughout the material implies the FENG loudspeaker sensitivity is proportional to the thickness of the FENG sheet.

4.2. Point approximation source

Based on dimensions of the FENG and the acoustic wavelength that it creates, it can be classified to behave as a point source (radiates sound uniformly in all directions). The conditions of this is that $kL \ll 1$ where $k = \omega/c$ and L is the longest dimension

of the FENG. Under these conditions the pressure at a given distance r is given by:

$$p(r,t) = \frac{i\omega\rho}{4\pi} \frac{u}{r} e^{i(\omega t - kr)},\tag{3}$$

where:

p is the pressure in Pascal;

u is the volume velocity in m^3/s ;

 ω is the angular frequency in rad/s;

k is the wavenumber = ω/c where c is the speed of sound (343.2 m/s);

r is the distance from the source to the observation point in meters;

 ρ is the density of air (1.18 kg/m³);

The volume velocity (u) is equal to the area (A) of the FENG times its velocity. Since the velocity is the time derivative of the displacement, a FENG of thickness (D) responding to an applied sinusoidal voltage (V) would have a 2-sided (both front and back) volume velocity of:

$$u = i\omega DR_{\nu}VA$$
. (4)

Equation (3) then becomes:

$$p(r,t) = -DR_{\nu}AV\frac{\omega^{2}\rho}{4\pi r}e^{i(\omega t - kr)}.$$
(5)

Equation (5) reveals that the pressure is: 1) linearly proportional to the FENG area; 2) linearly proportional to the thickness; 3) proportional to the square of the frequency.

This theory supports the results produced by the multilayer FENG and FENGs frequency response.

4.3. Estimating the change in thickness of the FENG

The SPL (sound pressure level) is 20 times the logarithm of ratio of measured effective sound pressure (rms) to reference effective sound pressure. This reference sound pressure is 2×10^{-5} Pa. Thus, by knowing the SPL output of the FENG at given frequency and measured from a given distance, the change in thickness of the FENG can be computed. The expression for pressure from point source approximation, converting that to SPL would be

$$SPL = 94 + 20\log_{10} \frac{\rho d\omega^2 L^2}{4\sqrt{2}\pi r}.$$
 (6)

From the collected data, SPL was 50 dB at a frequency of 2000 Hz at a distance of 30 cm. The frequency of 2000 Hz is chosen because the noise is minimum, although it is outside the domain of validity of the model (for the smallest FENG) by 180 Hz –note that for FENG of side 3 cm, kL = 1 at 1820 Hz. Substituting these values into equation (6) results in a peak displacement of 28 nm. The FENG thickness is 78 μ m, so the relative change in FENG thickness is 0.04%.

4.4. High frequency general model

As *kL* approaches unity, the simple low frequency model no longer holds, and more sophisticated methods must be used. Analytical solutions for these methods exist only for the simplest cases and it will be necessary to rely on numerical solutions to compare with measurements. One of these methods uses the Kirchhoff–Helmholtz integral equation [28] and can be used to solve for the acoustic pressure anywhere upon, or in the space surrounding the FENG at any frequency. The method accounts for the effects of scattering, diffraction and shading. The equation is:

$$\phi(\mathbf{r}) = \phi_{ext}(\mathbf{r}) + \int_{S} \left[G(\mathbf{r}, \mathbf{r}') \mathbf{v}(\mathbf{r}') - \phi(\mathbf{r}') \nabla G(\mathbf{r}, \mathbf{r}') \right] \cdot d\mathbf{S}, \tag{7}$$

where $\phi(\mathbf{r})$ is the acoustic potential measured at the point \mathbf{r} . It is related to the pressure: $p(r) = i\omega\rho\phi(\mathbf{r})$; $\phi_{ext}(\mathbf{r})$ is the total potential at the point \mathbf{r} due to all the external sources; $\mathbf{v}(\mathbf{r}') = \nabla\phi(\mathbf{r}')$ is the particle velocity; $G(\mathbf{r},\mathbf{r}')$ is the Green's function for acoustics given by:

$$G(\mathbf{r}, \mathbf{r}') = \frac{e^{ik|\mathbf{r} - \mathbf{r}'|}}{4\pi |\mathbf{r} - \mathbf{r}'|}.$$
 (8)

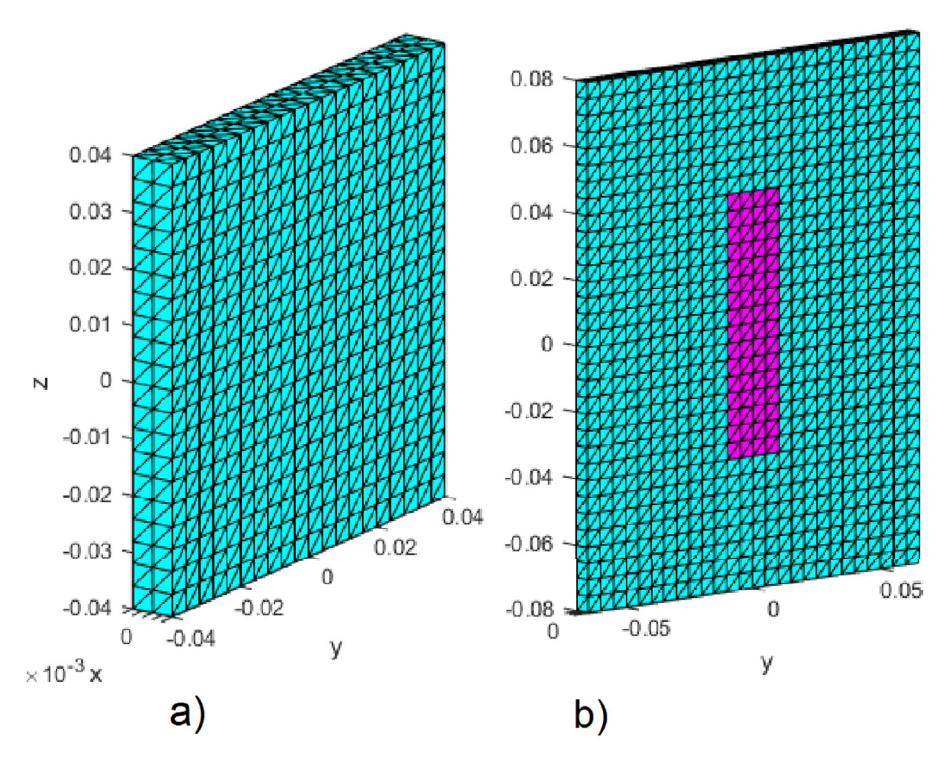


Fig. 11. Discretization of FENG surface for simulations.a) When the FENG is of the same size as the back-plate b) Discretization of the model with FENG (pink color) on a back-plate smaller (blue color) than its size. (For interpretation of the references to color in this figure legend, the reader is referred to the Web version of this article.)

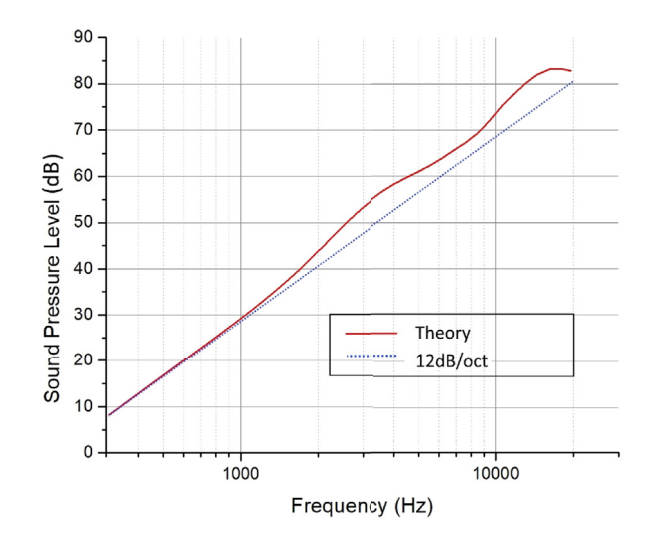


Fig. 12. Simulation results for a square FENG with a solid back-plate the same size as the FENG; showing the frequency response at 30 cm in front of the FENG.

4.5. Model accounting for solid back-plate

The FENG was measured when fixed to a solid back-plate. This removes the symmetry leading to the simpler Rayleigh equation. When there is no symmetry in the model which prevents diffraction and reflection, the full weight of the Kirchhoff–Helmholtz integral equation (7) must be used. A numerical solution to the equation is embodied in the "Boundary Element Method" (BEM) which involves the following steps:

1) Discretize the surface into N elements sufficiently small that the potential can be approximated by a simpler function. The surface integrals in Equation (7) can then be evaluated numerically over each element separately. The entire surface integral is the sum of the integrals over each element.

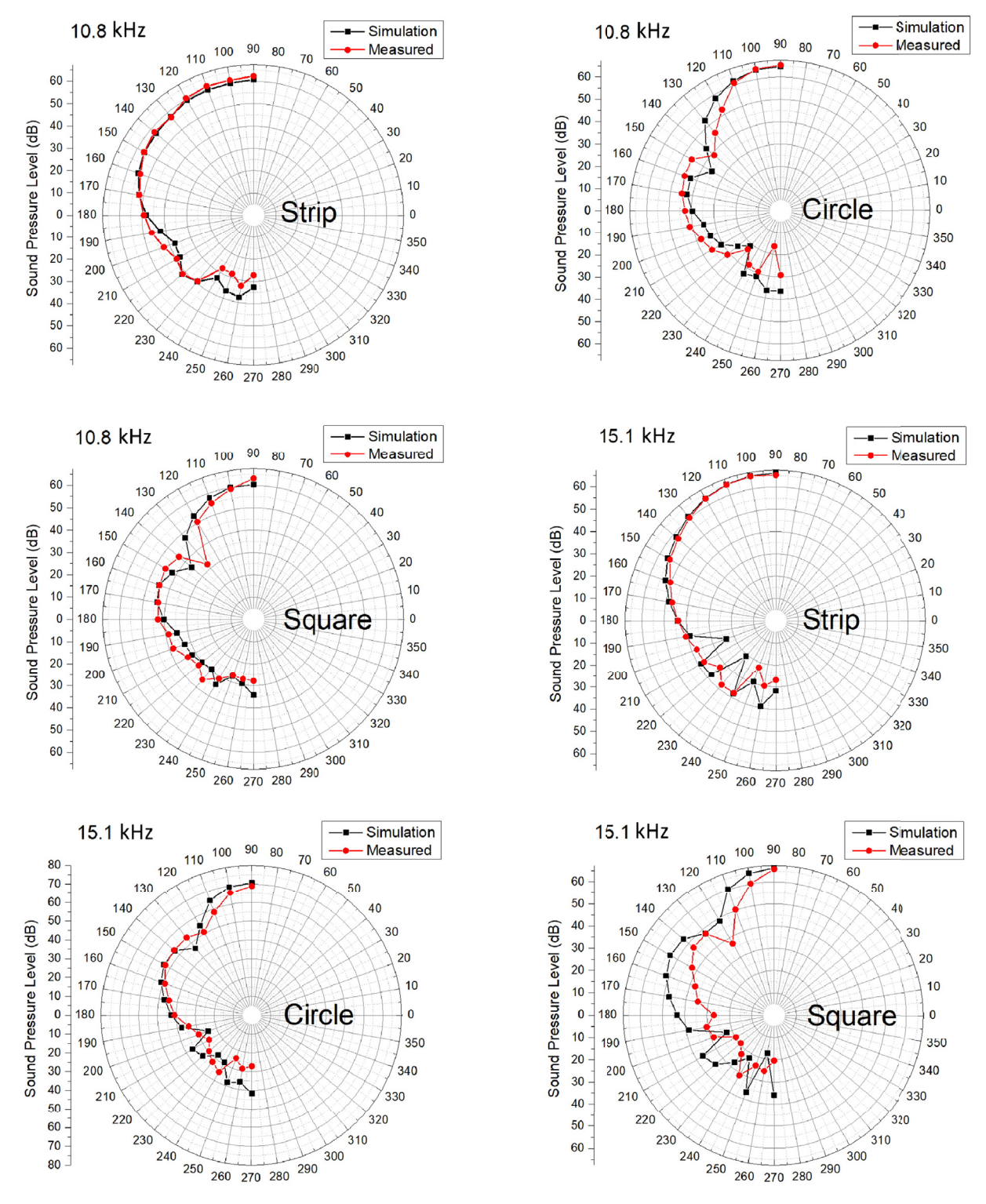


Fig. 13. Simulation results are compared with corresponding measurements.

- 2) Apply Equation (7) N times, each time with \mathbf{r}' at the centroid of a different element. This step results in N equations and 2N unknowns: N unknown values of ϕ (one at each element centroid) and N unknown values of \mathbf{v} .
- 3) The N equations resulting from step 2 are assembled into a matrix equation. The boundary conditions are applied at each element to eliminate either ϕ or \mathbf{v} .

- 4) The matrix equation is solved (e.g. with Gaussian Elimination methods) resulting in values for ϕ and \mathbf{v} for every element on the surface.
- 5) Having solved for the velocity potential and its derivative on the surface, the last step is to again apply Equation (7) to solve for the potential (or the velocity) anywhere in the solution domain.

The discretization of the FENG into triangular elements for this calculation is shown Fig. 11.

The frequency response at a position perpendicular to the FENG plane and 30 cm from it is shown in Fig. 12. The back-plate is the same size as the FENG and is 0.5 inches thick. There are a few expected features reproduced by the theory of a square FENG of side *L*:

- 1) At low frequencies where $L \ll \lambda$, the frequency response rises at 12 dB/octave.
- 2) When $L \approx \lambda$, the response starts to rise above 12dB/octave as the radiator gets more directional and less energy gets sent backward.
- 3) When $L \gg \lambda$ the maximum boost of 6 dB is reached and the response continues to rise at 12 dB/octave.
- 4) There is some waviness due to diffraction. This happens when the FENG side length are multiples of wavelength.

The experiments were performed on FENG devices mounted on back-plates (MDF) that were larger than the FENG (see Fig. 2). The model for this (in the case of a rectangular strip) is shown in Fig. 11b.

Simulation was carried out for different shapes. Selected results are overlaid with measurements as shown in Fig. 13. It can been seen that for various shapes at various frequencies the directivity pattern measured is in close correlation to the simulation. It must be noted that the SNR on the back side of the FENG $(180^{\circ} - 270^{\circ})$ is poorer compared to the front side $(90^{\circ} - 180^{\circ})$.

5. Conclusion

A BEM model was developed and showed close correlation to experimental data. The studies in this work show that the Sound Pressure Level (dB) of a FENG device, when used as a loudspeaker, increases at the rate of 12 dB/octave; and the Sound Pressure (Pa) increases linearly with addition of layers and surface area. Thus, increasing the output Sound Pressure of FENG devices used as loudspeakers can be achieved by stacking layers connected electrically in parallel and increasing the loudspeaker's area. For a 16 cm² FENG, the output increases from 40 dB to % 52 dB at around 3 kHz by stacking 4 layers. As expected, the output also increases linearly with the amplitude of the input signal. Directivity can be controlled by the loudspeaker's geometrical shape. It is shown that a strip is the least directional shape in comparison with 3 other shapes tested. For further improvements, the option of increasing the dipole density during fabrication steps can be explored, along with various other electrode materials, thereby improving the R_{ν} of the FENG, which is expected to increase the output Sound Pressure.

Acknowledgements

This work was supported by the National Science Foundation (NSF ECCS Award: ECCS-1854750) and Ford Motor Company.

Appendix A. Variables and Constants

- 1. R_{v} is the intrinsic response, which is the fractional change in FENG thickness per applied Volt in units of V^{-1} ;
- 2. *P*, *p* are pressure in units of Pa;
- 3. u is the volume velocity in units of m^3/s ;
- 4. ω is the angular frequency in units of rad/s;
- 5. *k* is the wavenumber = ω/c , where *c* is the speed of sound in air (343.2 m/s);
- 6. *r* is the distance from the source to the observation point in unites of m;
- 7. ρ is the density of air (1.18 kg/m³);
- 8. *D* is the thickness of the FENG in units of m;
- 9. $\phi(\mathbf{r})$ is the acoustic potential measured at the point \mathbf{r} .

References

- [1] F. Casset, J. Danel, P. Renaux, C. Chappaz, F. Bernard, T. Sednaoui, S. Basrour, B. Desloges, S. Fanget, 4-inch transparent plates based on thin-film AlN actuators for haptic applications, Mechatronics 40 (2016) 264–269, https://doi.org/10.1016/j.mechatronics.2016.05.014.
- [2] B.J. Park, S. Park, S. Yun, S. Nam, K.-U. Kyung, A transparent visuo-haptic input device with optical waveguide based thin film display, sensor and surface actuator, Sens. Actuators A Phys. 233 (2015) 47–53, https://doi.org/10.1016/j.sna.2015.06.028.
- [3] J. Rowland, Flexible audio speakers for composition and art practice, Leonardo Music J. 23 (2013) 33-36, https://doi.org/10.1162/LMI_a_00151.
- [4] S. Kang, S. Cho, R. Shanker, H. Lee, J. Park, D.-S. Um, Y. Lee, H. Ko, Transparent and conductive nanomembranes with orthogonal silver nanowire arrays for skin-attachable loudspeakers and microphones, Sci. Adv. 4 (8) (2018) eaas8772.
- [5] F. Sorgini, A. Mazzoni, L. Massari, R. Cali, C. Galassi, S.L. Kukreja, E. Sinibaldi, M.C. Carrozza, C.M. Oddo, Encapsulation of piezoelectric transducers for sensory augmentation and substitution with wearable haptic devices, Micromachines 8 (9) (2017) 270, https://doi.org/10.3390/mi8090270.

- [6] Y. Gao, R. Chandrawanshi, A.C. Nau, Z.T.H. Tse, Wearable virtual white cane network for navigating people with visual impairment, Proc. Instit. Mech. Engineers., Part H: J. Eng. Med. 29 (9) (2015) 681–688, https://doi.org/10.1177/0954411915599017.
- [7] C. Habib, A. Makhoul, R. Darazi, R. Couturier, Health risk assessment and decision-making for patient monitoring and decision-support using Wireless Body Sensor Networks, Inf. Fusion 47 (2019) 10–22, https://doi.org/10.1016/j.inffus.2018.06.008.
- [8] J.M. Eargle, Cone and dome drivers, in: Loudspeaker Handbook, Springer, Boston, MA, 1999, pp. 21-46, https://doi.org/10.1007/978-1-4615-7361-6_2.
- [9] J.M. Eargle, In-line and planar loudspeaker arrays, in: Loudspeaker Handbook, Springer, Boston, MA, 1999, pp. 114-135, https://doi.org/10.1007/978-1-4615-7361-6_6.
- [10] C. Dagdeviren, P. Joe, O.L. Tuzman, K.-I. Park, K.J. Lee, Y. Shi, Y. Huang, J.A. Rogers, Recent progress in flexible and stretchable piezoelectric devices for mechanical energy harvesting, sensing and actuation, Extreme Mech. Lett. 9 (2016) 269–281.
- [11] Z. Zhao, C. Shuai, Y. Gao, E. Rustighi, Y. Xuan, An application review of dielectric electroactive polymer actuators in acoustics and vibration control, J. Phys.: Conf. Ser. 744 (2016) 012162 IOP Publishing.
- [12] X. Yu, R. Rajamani, K. Stelson, T. Cui, Carbon nanotube-based transparent thin film acoustic actuators and sensors, Sens. Actuators A Phys. 132 (2) (2006) 626–631, https://doi.org/10.1016/J.SNA.2006.02.045.
- [13] H. Zhu, X. Yu, R. Rajamani, K. Stelson, Active control of glass panels for reduction of sound transmission through windows, Mechatronics 14 (7) (2004) 805–819.
- [14] Y. Kaijun, L. Lin, M. Ichchou, M. Collet, Sound insulation performance of plates with interconnected distributed piezoelectric patches, Chin. J. Aeronaut. 30 (1) (2017) 99–108, https://doi.org/10.1016/j.cja.2016.12.012.
- [15] M. Sharifzadeh Mirshekarloo, C.Y. Tan, X. Yu, L. Zhang, S. Chen, K. Yao, F. Cui, S.M. Pandit, S.H. Chong, S.T. Tan, Transparent piezoelectric film speakers for windows with active noise mitigation function, Appl. Acoust. 137 (2018) 90–97, https://doi.org/10.1016/j.apacoust.2018.03.017.
- [16] B. Aloufi, K. Behdinan, J. Zu, Vibro-acoustic model of an active aircraft cabin window, J. Sound Vib. 398 (2017) 1–27, https://doi.org/10.1016/j.jsv.2017.03.
- [17] P. Rothemund, X.P. Morelle, K. Jia, G.M. Whitesides, Z. Suo, A transparent membrane for active noise cancelation, Adv. Funct. Mater. 28 (29) (2018) 1800653https://doi.org/10.1002/adfm.201800653.
- [18] N. Arora, S.L. Zhang, F. Shahmiri, D. Osorio, Y.-C. Wang, M. Gupta, Z. Wang, T. Starner, Z.L. Wang, G.D. Abowd, Saturn: a thin and flexible self-powered microphone leveraging triboelectric nanogenerator, Proc. ACM Interact., Mob., Wearable Ubiquitous Technol. 2 (2) (2018) 60.
- [19] I. Graz, M. Kaltenbrunner, C. Keplinger, R. Schwdiauer, S. Bauer, S.P. Lacour, S. Wagner, Flexible ferroelectret field-effect transistor for large-area sensor skins and microphones, Appl. Phys. Lett. 89 (7) (2006) 073501.
- [20] H. Guo, X. Pu, J. Chen, Y. Meng, M.-H. Yeh, G. Liu, Q. Tang, B. Chen, D. Liu, S. Qi, et al., A highly sensitive, self-powered triboelectric auditory sensor for social robotics and hearing aids, Sci. Robot. 3 (20) (2018) eaat2516.
- [21] W. Li, D. Torres, T. Wang, C. Wang, N. Seplveda, Flexible and biocompatible polypropylene ferroelectret nanogenerator (feng): on the path toward wearable devices powered by human motion, Nano Energy 30 (2016) 649–657.
- [22] Y. Cao, W. Li, J. Figueroa, T. Wang, D. Torres, C. Wang, Z.L. Wang, N. Seplveda, Impact-activated programming of electro-mechanical resonators through ferroelectret nanogenerator (feng) and vanadium dioxide, Nano Energy 43 (2018) 278–284.
- [23] B. Rakerd, E.J. Hunter, M. Berardi, P. Bottalico, Assessing the acoustic characteristics of rooms: a tutorial with examples, Perspect. ASHA Special Interest Groups 3 (19) (2018) 8–24.
- [24] W. Li, D. Torres, R. Daz, Z. Wang, C. Wu, C. Wang, Z. Lin Wang, N. Seplveda, Nanogenerator-based dual-functional and self-powered thin patch loudspeaker or microphone for flexible electronics, Nat. Commun. 8 (2017), https://doi.org/10.1038/ncomms15310 1531015310.
- [25] D.K. Hsu, Nondestructive testing using air-borne ultrasound, Ultrasonics 44 (2006) e1019–e1024.
- [26] T. Zweschper, A. Dillenz, G. Riegert, D. Scherling, G. Busse, Ultrasound excited thermography using frequency modulated elastic waves, Insight-Non-Destruct. Test. Condition Monit. 45 (3) (2003) 178–182.
- [27] X. Guo, V. Vavilov, Crack detection in aluminum parts by using ultrasound-excited infrared thermography, Infrared Phys. Technol. 61 (2013) 149–156.
- [28] L.C. Wrobel, The Boundary Element Method, Applications in Thermo-Fluids and Acoustics, vol. 1, John Wiley & Sons, 2002.